Int. J. Heat Mass Transfer. Vol. 35, No. 4, pp. 795–801, 1992
Printed in Great Britain

0017–9310/92 $5.00 + 0.00

Heat transfer in an overhead electrical conductor

S. H. LIN
Department of Chemical Engineering, Yuan Ze Institute of Technology, Neili, Taoyuan, Taiwan 32026, China

(*Received* 15 *March* 1991 *and in final form* 6 *May* 1991)

Abstract—A heat transfer model is presented to describe the thermal responses of an overhead electric conductor in a high voltage power transmission line when subjected to changes in operating and ambient conditions. The thermal model takes into account all major heat transfer mechanisms happening to the conductor in a natural environment. The original heat transfer and simplified macroscopic models are employed to predict the conductor temperature distributions under various indoor and outdoor operating conditions. Good agreement between the theoretical predictions and the observed data justifies the various assumptions involved in the development of the simplified macroscopic model.

1. INTRODUCTION

HIGH VOLTAGE power transmission towers are common along highways and/or in remote areas. These tall steel towers are an integral part of high voltage power transmission systems. Heat transfer plays a vital role in the whole power transmission system. In fact, high voltage power transmission is a highly thermal limiting process. An overhead conductor, which usually consists of numerous aluminum or copper strands, produces a large quantity of heat due to resistive heating. High conductor temperature can produce two unwanted physical characteristics: sag and annealing [1, 2]. The sag of a conductor increases with increasing temperature because of expansion of the material. Conductor sag is a reversible process providing the yield strength of the materials has not been exceeded. Two aging phenomena common to conductors are annealing and creep. These phenomena lead to direct loss of strength of the conductor with time. The rate at which a conductor anneals and creeps increases as the conductor temperature increases. Unlike conductor sag, conductor annealing and creep are irreversible processes. A utility company usually wants to maximize the load of the line without thermally overburdening it. It is therefore important for a utility company to know the conductor temperature in a high voltage power transmission system.

Many articles have been published in establishing the relationship between the conductor temperature and the electric current that a transmission line can carry [1–6]. More recently, Sluzalec [7] presented a thermal model for predicting the conductor temperature under cyclic current load conditions. It is somewhat idealized because many important environmental factors that affect the thermal responses of an overhead conductor were not considered. In addition, the cyclic current load used in his model is not the usual operating mode of high voltage power transmission. In the present study, two more realistic models are presented. The first model takes into consideration many important operating and environmental factors which affect the conductor thermal responses, while the second one represents a simplification by assuming the conductor radial temperature gradient to be in a quasi-steady state. Indoor and outdoor experimental tests were conducted to gather the conductor surface temperature data which are employed to verify the model proposed.

2. THERMAL MODEL OF AN ELECTRIC CONDUCTOR

Figure 1 shows a typical aluminum conductor steel reinforced (ACSR) conductor [8]. The inner core steel strands are used for strength and carry practically no electric current. Therefore, the temperatures within these steel strands are relatively uniform because very little resistive heat is generated. The electric current of the conductor is primarily carried by the outer aluminum strands. Table 1 lists some important characteristics of the Drake 795 kcmil 26/7 ACSR conductor [8], which is frequently used on the 240 kV transmission line and is capable of carrying over 1200 A of current, although it is normally rated at a lower load.

The basic heat transfer mechanisms occurring in a conductor consist of the resistive heat generation in the aluminum strands, heat conduction through the aluminum strand matrix, natural or forced convection from the conductor surface to the ambient air, radiation heat loss from the conductor surface and solar radiation absorbed by the conductor. The transient conductor thermal model can be represented by the following equation:

$$\rho C_p \frac{\partial T}{\partial t} = k_r \left(\frac{\partial^2 T}{\partial r^2} + \frac{1}{r} \frac{\partial T}{\partial r} \right) + S_e(T) \qquad (1)$$

where $S_e(T)$ is the resistive heat generation and k_r the

NOMENCLATURE

a, b	constant parameters in the electrical resistance equation
A	aluminum conductor cross-sectional area
B	conductor age
C_p	conductor specific heat
h	surface convection transfer coefficient
h_r	radiative heat transfer coefficient
I	conductor current
k	air thermal conductivity
k_r	effective thermal conductivity of conductor
Nu	overall Nusselt number, $2R_o U/k_r$
Nu'	convective Nusselt number, $2R_o h/k_r$
Q_s	solar heating absorbed by conductor
r	radial coordinate
Ra	Rayleigh number, $8g\beta R_o^3\rho (T_s - T_a) C_p/k\eta$
R_{ac}	conductor electrical resistance
Re	Reynolds number, $2R_o V/\eta$
R_i	inner conductor radius
R_o	outer conductor radius
S_a	constant parameter in solar heating equation
S_c	resistive heating
t	time
T	conductor temperature
T_a	air temperature
T_c	mean conductor temperature
T_i	aluminum/steel interface temperature
T_s	conductor surface temperature
T_0	initial conductor temperature
U	overall heat transfer coefficient
V	wind speed
w	wind angle.

Greek symbols

β	thermal expansion coefficient of air [K^{-1}]
ε	dimensionless radial coordinate, r/R_o
ε_i	ratio of inner to outer radii of conductor, R_i/R_o
ε_s	solar absorptivity/emissivity
η	kinematic viscosity of air
μ	apparent viscosity of air
ρ	conductor density
ρ_a	air density
σ	Boltzmann constant.

effective thermal conductivity of the conductor. It is implicitly assumed that the heat conduction in the conductor occurs in the radial direction only. In reality, circumferential and axial temperature gradients may exist, but these temperature gradients were experimentally observed to be very small in comparison with that in the radial direction [6] and can be ignored. The initial and boundary conditions for equation (1) are represented by

$$t = 0, \qquad T = T_0 \tag{2a}$$

$$r = R_i, \qquad \frac{\partial T}{\partial r} = 0 \tag{2b}$$

$$r = R_o, \qquad k_r \frac{\partial T}{\partial r} = h(T_a - T). \tag{2c}$$

Subject to equations (2a)–(2c), equation (1) was integrated by an iterative implicit finite difference method [9].

In practice, real-time applications of equation (1) in predicting the conductor temperature in a high voltage transmission line involve simultaneous processing of a large amount of measured weather and conductor data. Rigorous solution of equation (1) by the implicit finite difference method requires a significant amount of computer time even on a mainframe computer. Hence simplification of equation (1) is often helpful in many practical applications.

Integrating equation (1) over the outer aluminum section of the conductor, the spatially dependent microscopic equation is transformed into a macroscopic form

$$\frac{dT_c}{dt} = \frac{1}{1-\varepsilon_i^2} \frac{2k_r}{\rho C_p R_o} \left(\frac{\partial T}{\partial r}\bigg|_{r=R_o} \right) + \frac{S_c(T_c)}{\rho C_p} \tag{3}$$

in which T_c is the mean conductor temperature. It is assumed here that there is no heat flux across the aluminum/steel interface. Mathematical integration leading to equation (3) also involves other sim-

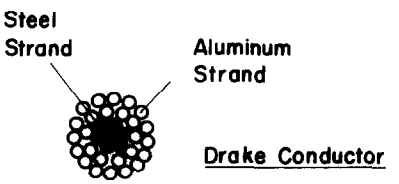

FIG. 1. Strand configurations of the Drake ACSR and copper conductors.

Table 1. Characteristics of the Drake ACSR conductor

No. of core steel strands	7
No. of aluminum strands	26
Conductor radius (cm)	1.4072
Inner steel core radius (cm)	0.5182
Aluminum strand radius (cm)	0.2223
Steel strand radius (cm)	0.1735

plifications. For example, the resistive heating $S_e(T_c)$ is evaluated at the mean conductor temperature T_c and is therefore assumed to be constant across the aluminum layers. This is certainly not exact, but is deemed adequate for the present application because the resistive heating is not very sensitive to the conductor temperature in the normal operating range of current load. The conductive heat flux term at the conductor surface can be obtained from the boundary condition

$$k_r \left.\frac{\partial T}{\partial r}\right|_{r=R_o} = -U(T_s - T_a) + Q_s. \tag{4}$$

Combination of equations (3) and (4) leads to

$$\frac{dT_c}{dt} = \frac{S_e(T_c)}{\rho C_p} - \frac{2U(T_s - T_a) - 2Q_s}{(1-\varepsilon_i^2)\rho C_p R_o}. \tag{5}$$

Equation (5) is a simplified macroscopic version and is much easier to integrate than the original partial differential equation, equation (1). However, this equation involves the conductor surface temperature (T_s) and the mean conductor temperature (T_c). These two temperatures are related by the radial temperature gradient of the conductor, which is still unknown. It is further assumed that the radial temperature gradient is in a pseudo-steady state. With this assumption, it is obtained from equation (1) that

$$\frac{d}{dr}\left(r\frac{dT}{dr}\right) = -\frac{S_e(T_c)r}{k_r}. \tag{6}$$

This can be integrated using the same boundary conditions and similar assumptions in deriving equation (5); we have

$$T - T_a = \frac{S_e R_o}{4k_r}\left[1 - \frac{2}{Nu} - \varepsilon^2 + 2\varepsilon^2\left(\ln\varepsilon + \frac{1}{Nu}\right)\right] + \frac{Q_s}{\pi U}. \tag{7}$$

Applying the above equation to the outer conductor surface and the aluminum/steel interface, respectively, yields

$$T_s - T_i = \frac{S_e(T_c)R_o}{4k_r}[1 - \varepsilon_i^2 + 2\varepsilon_i^2 \ln(\varepsilon_i)]. \tag{8}$$

Equation (8) permits calculation of the radial conductor temperature difference, $(T_s - T_i)$. Note that since T_c is involved in evaluating S_e, several iterations are needed in determining $(T_s - T_i)$ from equation (8). In conjunction with equation (8), equation (5) can be readily integrated to determine the transient conductor surface and interface temperatures.

The theoretical predictions of the conductor surface temperatures by the original model and the simplified model are compared with the measurements of indoor and outdoor tests in a later section.

3. CONDUCTOR THERMAL PROPERTIES AND HEAT TRANSFER CORRELATIONS

To apply the heat transfer equations given before, a few conductor thermal properties and heat transfer correlations are required. Foremost of all is the effective radial thermal conductivity of the conductor, k_r. As seen in Fig. 1, although the effective thermal conductivity may be estimated by the theoretical equation [9], the experimental values [10] are adopted here. Foss *et al.* [11] reported the effective thermal conductivities for several ACSR and copper conductors. They are in the range between 1.195×10^{-3} and 0.0167 cal $cm^{-1}\,°C^{-1}\,s^{-1}$ depending on the type of conductor. For the Drake ACSR conductor, which is of particular interest in the present study, the average effective thermal conductivity is about 3.345×10^{-3} cal $cm^{-1}\,°C^{-1}\,s^{-1}$.

The heat transfer coefficient from the outer conductor surface can be calculated from the Nusselt number, which in turn depends on weather, i.e. on whether the air flow is under the forced or natural convection condition. For forced convection, the Nusselt number is given by [11]

$$Nu' = 0.32 + 0.43Re^{0.52} \quad \text{for } Re < 1000 \tag{9a}$$

$$= 0.24Re^{0.6} \quad \text{for } Re > 1000 \tag{9b}$$

valid for air impinging on the conductor at right angles. In a real outdoor environment, the air can blow across the conductor at any angle between 0° and 90°. For a wind angle other than 90°, the Nusselt number or the convective heat transfer coefficient needs to be discounted by a factor. Davis [4] suggested the following empirical equation:

$$f(w) = 1.194 - \sin(w) - 0.194\cos(2w) + 0.368\sin(2w) \tag{10}$$

where w is the yaw or wind angle (0° for perpendicular wind and 90° for parallel wind). The net convective heat transfer coefficient is then the product of that computed from equation (9a) or (9b) and the discounting factor of equation (10). For free convection, the Nusselt number is represented by [11]

$$Nu' = 0.525Ra^{0.25} \tag{11}$$

where Ra is the Rayleigh number, which is the product of the Grashof number and the Prandtl number.

The transition between the free and forced convection is difficult to establish precisely and hence no definite heat transfer correlation is available. For the present study, the heat transfer coefficients for the free and forced convections were calculated when the wind speed was low. The larger coefficient was then adopted. For the ACSR conductors with a diameter between 1.27 and 3.81 cm, within which most popular

commercial ACSR conductors fall, the transition occurs at a wind speed of approximately 0.124 m s^{-1}.

In most circumstances, the conductor of a high voltage transmission line may run rather hot. At elevated temperature, the radiative heat loss can be a significant part of conductor heat dissipation. The radiative heat transfer coefficient can be computed from

$$h_r = \sigma\varepsilon_s \frac{(T_c+273)^4-(T_a+273)^4}{T_c-T_a} \quad (12)$$

where σ is the Stefan–Boltzmann constant and ε_s is the conductor emissivity, which is a function of conductor age because of surface oxidation of the aluminum strands and is given by [3]

$$\varepsilon_s = 0.23\frac{0.7B}{1.22+B} \quad (13)$$

B being the conductor age in years, assuming 10 years for the present study.

The solar radiation absorbed by the conductor is estimated based on the solar radiosity and the solar angle data given by House and Tuttle [2]:

$$Q_s = \varepsilon_a[2.111\cos(\pi/2-S_a)+0.373]\times 10^{-2} \quad (14)$$

where ε_a is the solar absorptivity of the conductor and can be represented similarly to the equation reported in ref. [12] except that the constant 0.23 is replaced by 0.13. The parameter S_a is given by

$$S_a = \pi/2[1-|12-t|/5] \quad (15a)$$

or

$$S_a = -0.1772 \quad \text{if } S_a < -0.1772 \quad (15b)$$

with t being the time. Equations (14), (15a) and (15b) are best fit to the data of House and Tuttle [2]. The empirical equation is adequate for computing the solar heat flux absorbed by the conductor.

The most important conductor heat source is the resistive heating S_e, represented by

$$S_e = DR_{ac}I^2/A \quad (16)$$

where R_{ac} is the electrical resistance, I the conductor current and A the total cross-sectional area of aluminum strands. The constant parameter D is the conversion factor (0.2388) which converts S_e to cal cm^{-3} s^{-1}. The electrical resistance is a linear function of conductor temperature as given by

$$R_{ac} = a+bT \quad (17)$$

where the constant parameters a and b are 6.58×10^{-7} Ω cm^{-1} and 2.809×10^{-9} Ω cm^{-1} $°C^{-1}$, respectively, for the Drake ACSR conductor. The parameter for other ACSR conductors can be found in ref. [8].

Other thermal properties of the aluminum and steel strands and air can be readily obtained from the standard reference book [12] and are not listed here.

4. INDOOR AND OUTDOOR EXPERIMENTAL TESTS

To verify the theoretical model presented in the previous section, an outdoor experimental set-up was erected, as depicted in Fig. 2. The Drake ACSR was employed in the test. The conductor was heated by the current transformer at the bottom of the conductor loop. The current within the conductor loop was measured by a Rogowski coil located near the current transformer. The conductor current could be adjusted between zero and 2000 A. This current was sufficient for attaining a conductor temperature over 125°C, which is the operating temperature limit imposed by the utility company on this conductor. The conductor surface temperatures of the test section (the horizontal span) were measured by three sets of thermocouples at different locations. One set of thermocouples was installed at the center of the test section with one set each side about 1 m from the conductor clamp. At each location, four thermocouples were soldered on the conductor surface 90° out of phase to each other. Small circumferential and axial temperature variations (within 3°C) were observed among the thermocouple readings. The conductor surface temperatures reported in the following figures represent the average of these measurements. A Weathertronic weather station was employed for measuring the weather data. It was positioned about 2 m beside the conductor loop and at the same height as the test section. Five variables were monitored in the experiment by a high speed Hewlett–Packard data acquisition system. The acquired data included the wind speed, wind angle, air temperature, current and conductor surface temperatures. Further details of the experimental apparatus can be found elsewhere [6].

A similar experimental set-up was also erected indoors. To provide the wind for this test, a bank of six fans was positioned about 3.5 m in front of the conductor loop 60° incidental to the test section of the conductor. The wind speed and wind angle were measured by the weather station before each test run. The indoor experimental runs were similar to those of the outdoor tests. The indoor tests allow the experimental conditions like the air temperature, solar radi-

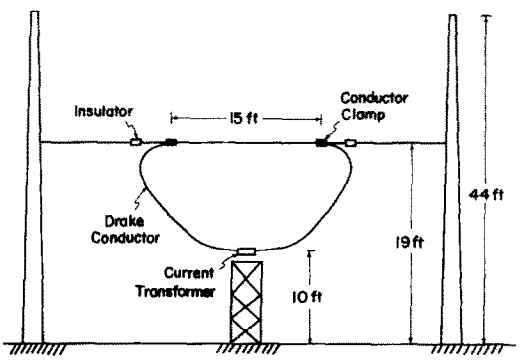

FIG. 2. Laboratory outdoor test facility.

ation, wind speed and wind angle to be controlled, whereas in the outdoor environment they are subject to the prevailing random weather conditions.

5. COMPARISON OF THEORETICAL AND EXPERIMENTAL RESULTS

Two indoor experimental results of step current change are shown in Figs. 3 and 4. In each test, an initial current of 600 A was applied to the conductor. At an ambient air temperature of 13°C, a steady state conductor surface temperature was established at 39°C under no wind conditions and maintained for over an hour. A step current change was then applied to the conductor and held constant for approximately 80 min which was sufficient for the conductor to establish a new steady state temperature under the no wind condition. Immediately following that, the fans were turned on, producing a constant 1.83 m s^{-1} wind speed at the test section of the conductor.

Figure 3 displays the results of the first indoor test run. The conductor surface temperature rises steadily after the step current change from 600 to 900 A is applied. When a constant wind speed of 1.83 m s^{-1} is applied, the conductor temperature is seen to drop rapidly, even below the original temperature level. The predicted conductor surface temperatures, as shown by the two continuous curves, compare rather well with the observations. As anticipated, the original model predicts the experimental data better than the simplified model. After the step current change, the conductor has a little delay in its thermal response because of the conductor thermal inertia. A similar delay appeared after the fans were turned on. The original model predicts this delay, but not the simplified macroscopic model which expects immediate conductor thermal response. However, the delay in the conductor's thermal response is relatively short such that the simplified model is deemed to be adequate considering the accuracy in the measured conductor surface temperatures in the experimental tests.

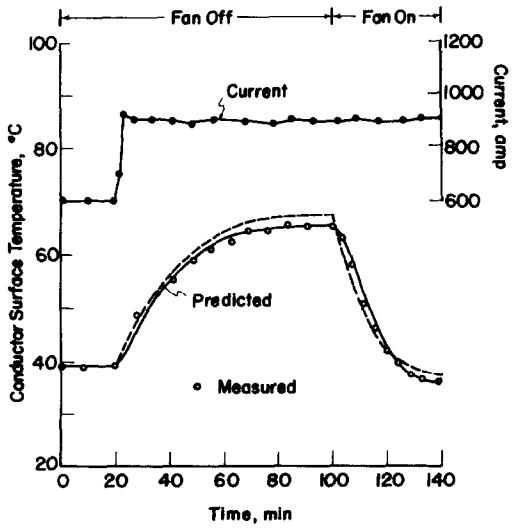

FIG. 3. Conductor temperature response to current transient from 600 to 900 A of indoor test. (———) Predicted by the original model. (- - - - -) Predicted by the simplified model.

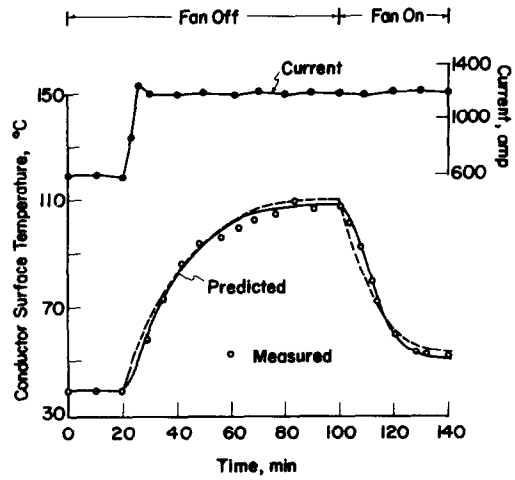

FIG. 4. Conductor temperature response to current transient from 600 to 1200 A of indoor test. (———) Predicted by the original model. (- - - - -) Predicted by the simplified model.

It is of interest to note that with wind, the conductor temperature rise after step current change is significantly slower than its fall after the fans are turned on. This indicates that the conductor responds much faster under wind conditions than under the no wind condition. An important parameter that characterizes the conductor's thermal response is the conductor time constant. The time constant, also known as the conductor response time, is defined as the time for the conductor to reach 63% of its new steady state temperature from the initial level. In other words, three time constants are generally sufficient for the conductor to establish a new steady state temperature. Figure 3 shows that without wind, the conductor time constant is about 20 min, whereas with 1.83 m s^{-1} wind, it decreases to about 6 min. Similar time constants have also been observed in other outdoor tests. In fact, the 20 min time constant establishes the upper extreme of the conductor response time. The other extreme of 1 or 2 min time constant has been observed when the wind is very strong, 10 m s^{-1} or even higher.

Figure 4 displays similar temperature response trends to those in Fig. 3. The conductor surface temperatures shown here are significantly higher than that in Fig. 3 because of the higher step current change applied to the conductor in the present case. The predicted conductor surface temperatures by both models are in good agreement with the observed values. The conductor time constants under wind and no wind conditions for this run are about the same as those of the previous one. This indicates that the conductor time constant is independent of the current load, as anticipated.

The result of the first outdoor experimental run is

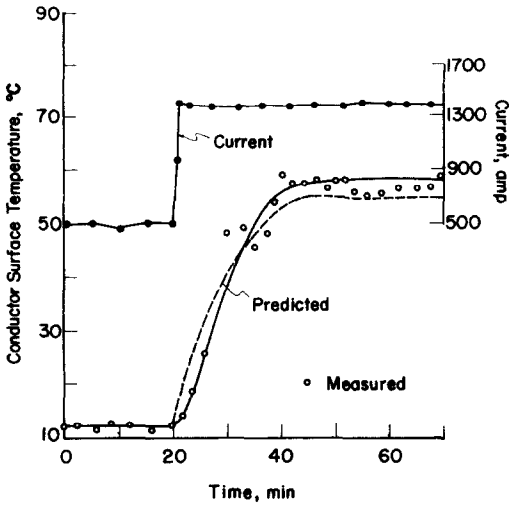

FIG. 5. Conductor temperature response to current transient from 980 to 1160 A of outdoor test. (———) Predicted by the original model. (- - - -) Predicted by the simplified model.

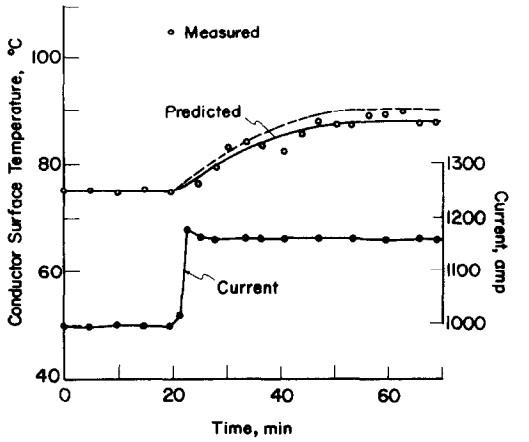

FIG. 6. Conductor temperature response to current transient from 500 to 1370 A of outdoor test. (———) Predicted by the original model. (- - - -) Predicted by the simplified model.

shown in Fig. 5. In this run, a constant initial current of 500 A was applied to the conductor loop for over an hour to establish an initial steady state conductor surface temperature at 19°C under the prevailing ambient air temperature of 6°C and wind speed fluctuating between 0.67 and 1.44 m s^{-1}. The conductor current was then elevated to 1370 A and held steady. The delay in the conductor's thermal response seems to be more pronounced in both outdoor runs. Part of the thermal response delay is caused by the conductor's thermal inertia. The fluctuating outdoor ambient may also have some influence. It is apparent in this figure that the measured conductor surface temperature is not as smooth as those of the indoor tests. This is obviously caused by the random fluctuations in the wind speed and wind angle in the outdoor environment. During the entire experimental period, the wind speed was observed to vary between 0.67 and 2.5 m s^{-1} with an average of 1.2 m s^{-1}. The wind angle varied between 0° and 83° with an average of 39° during the same period. Despite the random wind conditions, the model predictions by both models agree with the observed data reasonably well. The conductor time constant is more difficult to establish accurately for this run than the indoor one. Based on the predicted surface temperature curve, the time constant is estimated to be around 13 min, which is much larger than that of the indoor test with wind. This is primarily due to the lower average wind speed and wind angle.

Figure 6 shows another outdoor test result. In this case, the step current change was made from 980 to 1160 A. The air temperature was around 10°C and the wind speed between 0 and 1.14 m s^{-1}. The agreement between the measured and predicted conductor surface temperatures is also acceptable for this run. The conductor time constant is observed to be about 11 min for this run.

A typical measured radial conductor temperature gradient is shown in Fig. 7 as a function of the conductor current for the outdoor tests. Since the radial conductor temperature gradient is dependent on the ambient conditions, the data points in this figure show the general trend of the current effect. To really establish the relation between the radial conductor temperature gradient and the current, the ambient conditions need to be held constant. This implies that it can only be done in the indoor environment. The curve shows an exponential increase in the radial conductor temperature gradient with the conductor current. In most cases, the radial conductor temperature gradient is over 10% of the observed conductor surface temperature and can be as high as or even higher than 15% in many cases. Hence it is not reasonable to

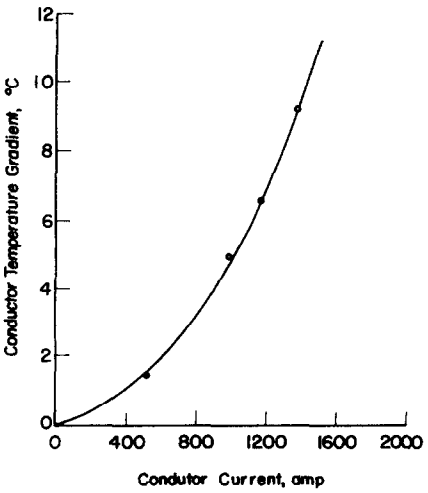

FIG. 7. Measured conductor temperature gradient as a function of the conductor current.

simply ignore the existence of the radial temperature gradient in the heat transfer model.

6. CONCLUSIONS

Two heat transfer models are presented in this study for predicting the thermal responses of an overhead electrical conductor in the high voltage transmission line. The original transient one-dimensional heat transfer model is integrated by an implicit finite difference method for predicting the conductor temperature distribution. It is also simplified to a macroscopic form by assuming the conductor radial temperature gradient to be in a quasi-steady state. Such a simplification is very useful because of the requirement of fast conductor temperature prediction for real-time applications of the heat transfer model. Several indoor and outdoor experimental tests using a typical Drake ACSR conductor are performed to verify the original and the simplified models. It has been found that, in comparison with the observed data, both model predictions are rather good even in the highly fluctuating outdoor environments. This clearly indicates that the simplified heat transfer model is adequate for predicting the conductor temperature under most practical circumstances.

Acknowledgement—The author wishes to acknowledge the financial support of this study by the National Science Council (NSC79-0402-E155-01), Taiwan.

REFERENCES

1. J. H. Wagborne and V. E. Ogorodnikov, Current carrying capacity of ACSR conductors, *AIEE Trans.* **70,** 1159 (1951).
2. H. E. House and P. D. Tuttle, Current-carrying capacity of ACSR, *AIEE Trans.* **77,** 1169 (1958).
3. Anonymous, Tailor conductor thermal ratings to need, *Elect. World* 34 (May 1976).
4. M. W. Davis, A new thermal rating approach : the real time thermal rating system for strategic overhead conductor transmission line. Part I, *IEEE Trans.* **PAS-96,** 803 (1977) and Part II, *IEEE Trans.* **PAS-96,** 810 (1977).
5. V. T. Morgan, The thermal rating of overhead line conductors, *Elect. Pwr Syst. Res.* **15,** 287 (1983).
6. S. D. Foss, S. H. Lin and R. A. Fernandes, Dynamic thermal line ratings : Part I, *IEEE Trans.* **PAS-102,** 1858 (1983) and Part II, *IEEE Trans.* **PAS-102,** 1865 (1983).
7. A. Sluzalec, Thermal phenomena in conductor, *Int. Commun. Heat Mass Transfer* **16,** 159 (1989).
8. *Aluminum Electrical Conductor Handbook*. The Aluminum Association, New York (1971).
9. L. Lapidus, *Digital Computation for Chemical Engineers*. McGraw-Hill, New York (1962).
10. S. C. Cheng and R. I. Vachon, The prediction of the thermal conductivity of two or three phase solid heterogeneous mixtures, *Int. J. Heat Mass Transfer* **12,** 249 (1969).
11. S. D. Foss, S. H. Lin and R. Carberry, Significance of conductor temperature difference with dynamic thermal rating methodology, *IEEE Trans.* **PWRD-2,** 502 (1987).
12. *General Electric Heat Transfer Data Book*. GE Corporate Research and Development, Schenectady, New York (1984).
13. R. E. Perry and C. H. Chilton, *Chemical Engineering Handbook* (5th Edn). McGraw-Hill, New York (1973).

TRANSFERT THERMIQUE DANS UN CONDUCTEUR ELECTRIQUE AERIEN

Résumé—On présente un modèle thermique pour décrire les réponses thermiques d'un conducteur électrique aérien dans une ligne de transmission de puissance à haute tension sujette à des changements de conditions opératoires et ambiantes. Le modèle thermique tient compte de tous les mécanismes thermiques principaux qui peuvent survenir au conducteur dans un environnement naturel. On emploie le transfert thermique original et les modèles macroscopiques simplifiés pour prédire les distributions de température dans le conducteur pour des conditions opératoires variées. Un bon accord entre les prédictions théoriques et les données observées justifie les hypothèses variées posées dans le développement du modèle macroscopique simplifié.

WÄRMEÜBERGANG AN ELEKTRISCHEN FREILEITUNGEN

Zusammenfassung—Das hier vorgestellte Wärmetransportmodell dient zur Beschreibung des thermischen Verhaltens einer elektrischen Freileitung in einem Hochspannungsleitungsnetz unter dem Einfluß wechselnder Betriebszustände und Umgebungsbedingungen. Das thermische Modell berücksichtigt alle wichtigen Wärmeübertragungsmechanismen, denen eine Freileitung in natürlicher Umgebung ausgesetzt ist. Das ursprüngliche Wärmetransportmodell sowie vereinfachte makroskopische Modelle dienen zur Berechnung der Temperaturverteilung in der Leitung bei unterschiedlichen Betriebszuständen innerhalb und außerhalb von Gebäuden. Die gute Übereinstimmung zwischen den theoretischen Berechnungen und Meßwerten bestätigt die verschiedenen Annahmen die zur Erstellung des vereinfachten makroskopischen Modells verwendet wurden.

ТЕПЛОПЕРЕНОС В НАДЗЕМНЫХ ЭЛЕКТРОПРОВОДАХ

Аннотация—Предложена модель теплопереноса, описывающая тепловые характеристики надземного электропровода в высоковольтной электросети при изменяющихся режимах работы и внешних условиях. Тепловая модель учитывает все основные механиэзмы теплопереноса в электропроводе в естественных условиях окружающей среды. Предложенная модель теплопереноса и упрощенная макроскопическая модель используются для определения распределения температур в электропроводе при различных рабочих режимах внутри и вне помещения. Хорошее согласие между теоретическими расчетами и экспериментальными данными подтверждает правомерность различных предлоложений, используемых при разработке упощенной макроскопической модели.